1. Large Helical Device (LHD) Project

The Large Helical Device (LHD) project conducts fusion-grade confinement research in a steady-state machine to elucidate important research issues in physics and engineering for the helical-type fusion reactor. The LHD is one of the largest helical devices, with poloidal/toroidal period numbers of 2/10, and major and averaged plasma minor radius of 3.6 – 4.0 m and 0.6 m, respectively. A double helical coil and three pairs of poloidal coils are all superconducting, by which maximum magnetic field strength at the plasma center is 3 T. Twenty small normal conducting loop coils are equipped outside the cryostat to apply resonant magnetic perturbations to the plasma. For plasma heating, three negative-ion-based 180 – 190 keV neutral beams with total heating power of 8 – 16 MW are injected tangentially to the plasma. Two positive-ion-based 40 – 80 keV neutral beams with total heating power of 6 – 18 MW are also injected perpendicular to the plasma. In addition, electron cyclotron resonance heating with total heating power of ~ 5.5 MW is also available. For fuelling, LHD is equipped with four gas puff valves and two pellet injectors.

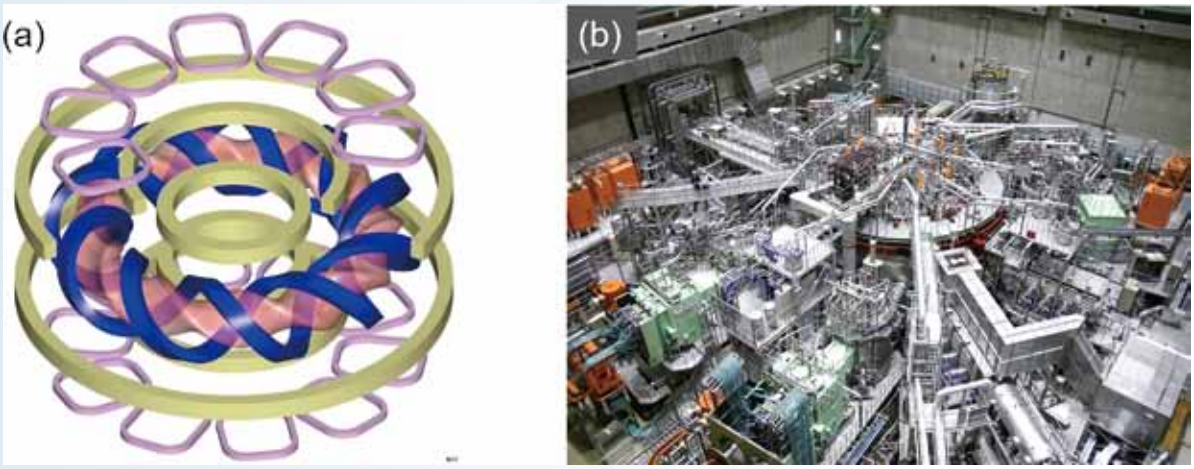

Fig. 1 (a) Coil configuration of LHD. Superconducting helical coils (blue), poloidal coils (yellow) and normal conducting RMP coils, together with plasma. (b) LHD torus hall.

In experiments conducted to date in tokamak devices, we have learned that plasma confinement performance is better in deuterium than in hydrogen, which is called the “isotope effect.” However, we do not yet understand clearly why plasma performance increases when we change the gas from hydrogen to deuterium. Clarifying the mechanism of this phenomenon is of great academic significance.
On March 7, 2017, LHD started the deuterium experiment, which successfully ended in August. The first experimental campaign with deuterium plasma produced a significant result. The ion temperature of 10 keV (120 million °C) was achieved.

Finally, achieved plasma parameters with hydrogen (before the deuterium experiment) are summarized in Table 1 with the targets of the LHD project.

Table 1 Achieved plasma parameters (1998 – 2017).

Parameters	Achieved	Key physics	Target
Ion temperature T_i	10 keV ($n_e = 1.2\times10^{19}$ m^{-3})	Ion ITB Impurity hole	10 keV ($n_e = 2\times10^{19}$m^{-3})
Electron temperature T_e	20 keV (2×10^{18} m^{-3}) 10 keV (1.6×10^{19} m^{-3})	Electron ITB	10 keV (2×10^{19}m^{-3})
Electron density n_e	1.2×10^{21}m^{-3} ($T_e = 0.25$ keV)	Super dense core	4×10^{20} m^{-3} ($T_e = 1.3$ keV)
Beta	5.1 % ($B_T = 0.425$ T) 4.1 % (1 T)	MHD in current-free plasmas	5 % ($B_T = 1$ - 2 T)
Duration time	54min. 28sec (0.5MW, 1keV, 4×10^{18}m^{-3}) 47min. 39sec. (1.2MW, 2keV, 1×10^{19}m^{-3})	Dynamic wall retention	1 hour (3 MW)

1. Large Helical Device (LHD) Project

Highlight

The ion temperature of 10 keV achieved, and the study on energetic particles progressed in the first LHD deuterium plasma experiment campaign

The deuterium plasma experiment was initiated in the LHD in March 2017. In its very first deuterium campaign, we successfully extended the high temperature regime in the LHD. The new record of the ion temperature (Ti) of 10 keV, which is the landmark achievement of helical systems research worldwide to satisfy one of fusion conditions. It was achieved with the ion internal transport barrier (ITB) formation, and several operational optimization [1]. The confinement characteristics of ITB plasmas were compared between hydrogen and deuterium discharges. The ion thermal diffusivity was reduced in the ion-ITB plasmas with deuterium compared with the plasmas without deuterium. It was also found that the electron thermal confinement of the electron-ITB plasmas was clearly improved in the deuterium case.
The study on energetic particles behaviour has been also extensively progressed in the first deuterium experiment campaign through the neutron measurement and consolidations of relevant simulation codes.

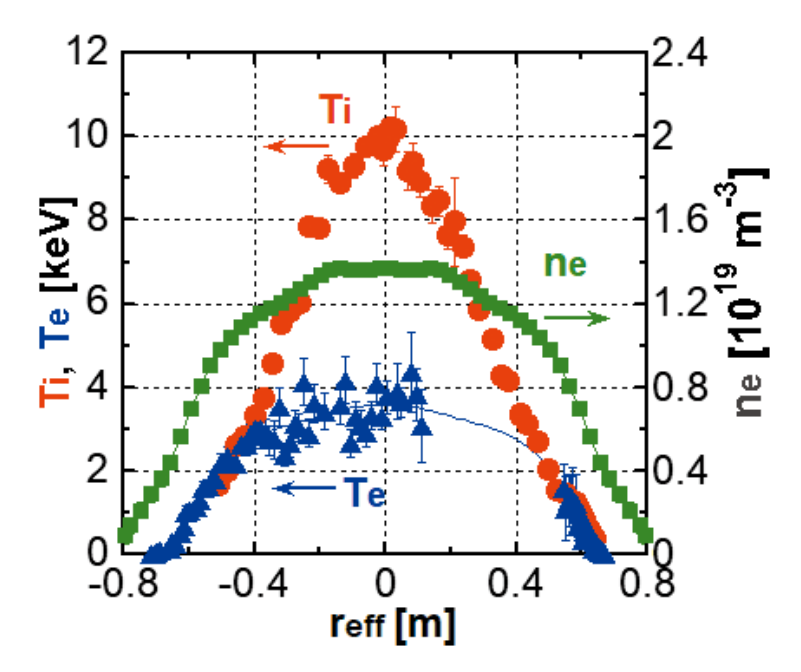

Fig. 1 The radial profiles of T_i, T_e, and n_e of the highest-T_i plasma in the LHD [reproduced from Y. Takeiri, Atoms 2018, 6(4), 69].

Extension of High-Temperature regime

During the first deuterium plasma experiment campaign, we achieved the highest T_i of 10 keV in the LHD due to the several operational optimizations such as the wall condition, the impurity quantity, and the magnetic configuration, with the increased NBI power [1]. Figure 1 shows radial profiles of T_i, T_e (electron temperature) and n_e (electron density) at the timing of the maximum T_i. The T_e and n_e data in 0.13 m < r_{eff} < 0.53 m were scattered due to the stray light from the in-vessel components, thus the data are omitted in Fig. 1. Slightly inward-shifted configuration of R_{ax} = 3.58 m /B_t = 2.87 T (counter clockwise direction) was chosen for the experiment. Also, the intensive wall conditioning using high power ECRH was conducted before the discharge. The plasma was sustained using high power NBI and the optimized-size carbon pellet was injected at t ~4.57 s. The central T_i was gradually increased after the additional NBI from t = 4.6 s and reached the maximum value at t = 4.85 s. The peaked T_i profile with the central value of 10 keV was successfully achieved. The achievement of the T_i of 10 keV is a milestone toward realizing a helical reactor, which has an intrinsic advantage for steady state operation, because the T_i value is one of the important ignition conditions.

The bursty MHD event, which is so-called energetic ion driven resistive interchange modes (EICs), was observed during the discharge. The EICs are driven by the increased pressure gradient of helically trapped energetic ions, which are mainly generated by the perpendicular NBI [2]. The neutron emission rate dropped associated with the EIC event. This indicates the loss of the energetic ions from the plasma. Consequently, the plasma stored energy and the ion temperature were degraded. Thus, the suppression of EICs is one of key issues for realizing higher-T_i plasmas in LHD. One of the control knobs of the EIC is ECRH. In the previous study, the EICs were found to be suppressed by an ECRH superposition [2]. On the other hand, the increase in the ion thermal diffusivity χ_i with increase in the T_e/T_i during the stepwise ECRH superposition was also observed in the LHD [3]. Higher T_i plasmas are possibly realized by suppressing EICs with a small increase in T_e/T_i using an optimized ECRH injection with moderate power and/or choosing the appropriate location of the ECRH power deposition with the off-axis ECRH injection.

Higher energy confinement in the high-T_e plasma with the strong e-ITB was also realized in the first deuterium experiment campaign in the LHD [1]. Figure 2 shows the radial profiles of (a) n_e, (b) T_e, and (c) the electron thermal diffusivity χ_e for H and D with approximately the same n_{e_fir} ~2.4×10^{19} m^{-3}. The magnetic configuration was R_{ax} = 3.6 m /B_t = 2.705 T (clockwise direction) both for the H and D plasmas. The purity of the target ions, $n_H/(n_H+n_D+n_{He})$, is 0.94 for the H-dominant plasma and 0.81 for the D plasma, respectively. Unfortunately, one gyrotron had trouble in the D experiment phase and thus that gyrotron was not available in this comparative experiment. Thus, the total ECRH injection power became smaller in the D-dominant experiments. Despite the decreased ECRH power for the D plasma, almost the same T_e profile with H plasma was realized. Although the n_{e_fir} was fixed as ~2.4×10^{19} m^{-3}, the n_e profile was slightly different between H and D plasma. The χ_e was evaluated from the power balance analysis and was decreased in r_{eff} < 0.3 m both for the H and the D plasma due to the formation of the e-ITB. From the comparison between these two cases, χ_e clearly reduced in the D plasma except for the plasma edge. The systematic data for the comparison of the global energy confinement of the e-ITB plasmas between H and D were also obtained with the n_{e_fir} of 1.5-4.7×10^{19} m^{-3} and the injection ECRH power of 1-3 MW. The energy confinement in D plasmas was found to be statistically 10-20% higher than H plasmas [5].

Progress of study on energetic particles behaviour

Global confinement property of beam ions is studied by means of the neutron flux monitor (NFM) since neutrons are primarily created by beam-plasma reaction in neutral beam (NB)-heated plasmas. An NB with the short pulse length, which is much shorter than Spitzer slowing down time, is injected into the magnetohydrodynamic (MHD)-quiescent electron-cyclotron-resonance-heated plasma in order to study whether or not beam ions slow down classically without beam ion loss. A rapid increase of total neutron emission rate (S_n) during NB injection and the slow decay of S_n following NB turn-off are observed. Numerical simulation using the 5D drift kinetic equation solver based on the Boozer coordinates, the Global NEoclassical Transport (GNET) code [6] shows that not only the decay time of S_n (τ_n) but also the absolute value of S_n agrees well with those obtained by experiment (Fig. 3). Hence, global beam-ion transport in LHD can be described in the neoclassical model in the MHD-quiescent regime.

As predicted by calculation based on Fokker-Planck equation [7], S_n increases with electron density (n_e) rapidly, then has a peak around n_e of around 2.5×10^{19} m^{-3}, and then decreases gently with n_e. Higher S_n in inward-shifted configuration are obtained and the maximum S_n reaches 3.3×10^{15} n/s in the first deuterium cycle. The line-integrated neutron profile is measured in co-injected NB-heated plasma with different magnetic axis (R_{ax}) with the vertical neutron camera (VNC). The neutron counts (C_n) become larger in the inward-shifted configuration, which is consistent with S_n. The radial peak position of C_n changes according to R_{ax} shows that the VNC works successfully as designed. Significant drop of C_n in central cords synchronized with a perpendicularly-injected-NB-excited MHD instability called helically-trapped EP driven resistive interchange mode (EIC) is observed. Note that S_n noticeably drops up to 50 % due to the EIC burst. By comparing the beam ion density predicted by the GNET code, the significant drop of C_n in central cords indicates

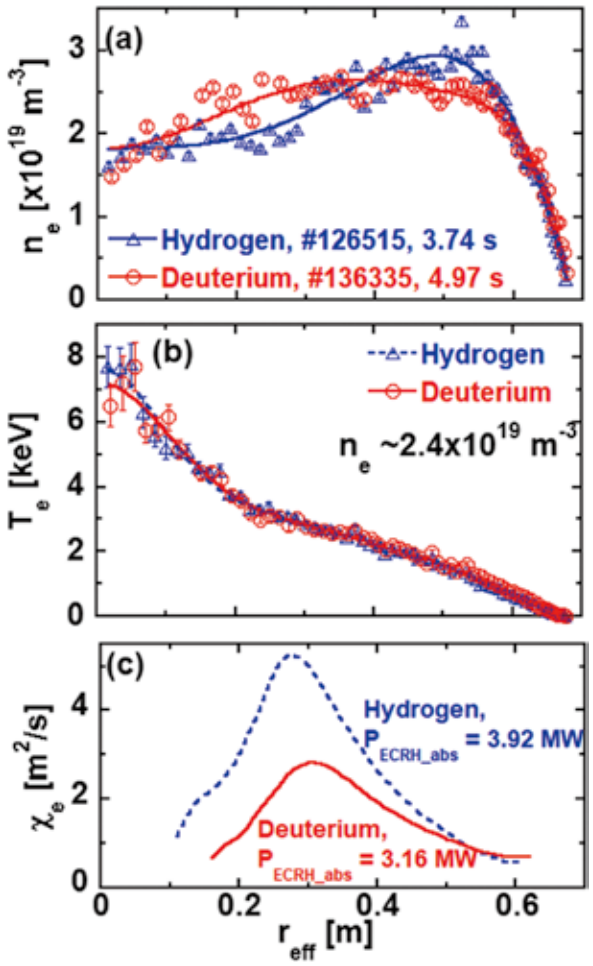

Fig. 2 The radial profiles of (a) n_e, (b) T_e, and (c) χ_e for H and D with approximately the same n_{e_fir} and the different ECRH power [1].

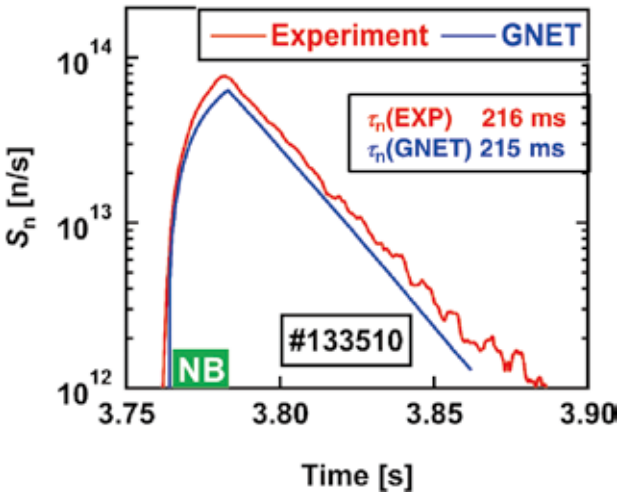

Fig. 3 Time evolution of S_n in a beam blip experiment. The time trend of S_n agrees with that calculated by the GNET simulation.

that helically-trapped beam ions are substantially lost due to the EIC.

Alpha particle simulation experiment is conducted by measuring 14 MeV neutron generated by secondary DT reactions in the deuterium plasma. Note that 1 MeV triton can be regarded as simulation particles of DT-produced alphas since kinematic parameters such as Larmor radius and processional drift frequency are quite similar. Time-resolved 14 MeV neutron flux is measured for the first time in stellarator/heliotron to study the confinement of 1 MeV triton produced by DD reaction using scintillating-fiber detectors calibrated with neutron activation systems. A build-up rate of 14 MeV neutron flux is slower than that of S_n as predicted according to the cross-section curves for DD and DT reactions. A significant increase of triton burnup ratio defined as a ratio of secondary DT neutron yield to primary DD neutron yield can be seen in the inward-shifted configuration (Fig. 4). The triton burnup simulation performed by the GNET code shows that the confinement of the helically-trapped tritons is improved by inward shift of R_{ax}.

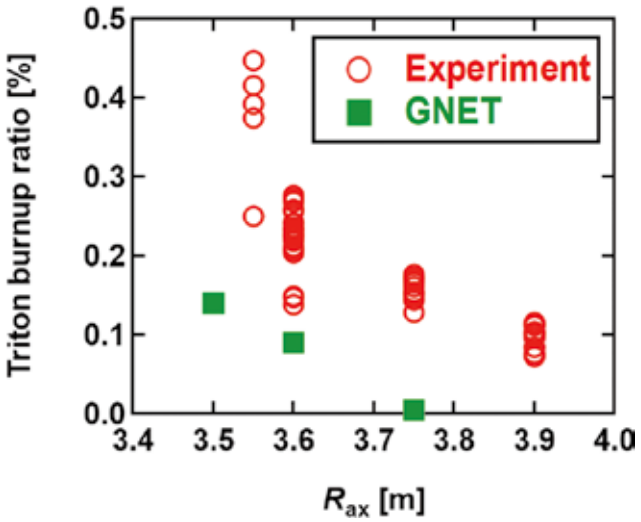

Fig. 4 Triton burnup ratio as a function of R_{ax}. The tendency is reproduced by the GNET simulation.

[1] H. Takahashi *et al.*, Nucl. Fusion **58** (2018) 106028.
[2] X.D. Du *et al.*, Phys. Rev. Lett. **118** (2017) 125001.
[3] H. Takahashi *et al.*, Nucl. Fusion **57** (2017) 086029.
[4] M. Nakata *et al.*, Comput. Phys. Commun. **197** (2015) 61.
[5] F. Warmer *et al.*, Nucl. Fusion **58** (2018) 106025.
[6] S. Murakami *et al.*, 2004 Fusion Sci. Technol. **46** (2004) 241.
[7] M. Osakabe *et al.*, 2017 Fusion Sci. Technol. **72** (2017) 199.

Highlight

Measurements of hydrogen-deuterium ratio in the core plasma with bulk charge exchange spectroscopy

Bulk charge exchange spectroscopy system has been installed in LHD to measure the radial profiles of $n_H/(n_H+n_D)$ and $n_D/(n_H+n_D)$ in the plasma from H_α and D_α lines emitted by the charge exchange reaction between the bulk ions and the neutral beam injected. The hot component due to the active charge exchange reaction with the neutral beam is smaller than the cold component emitted in the edge by one order of magnitude. In order to subtract the cold component of the H_α and D_α charge exchange lines, beam modulation technique is applied. Figure 1 shows the Spectrum of H_α and D_α lines after subtracting the spectrum at beam-off timing from the spectrum at beam-on timing for the discharge with H and D pellet injection. Although most of the cold components of the charge exchange lines are subtracted by the beam modulation, there still remain cold components comparable to the hot components, as seen in the spectra of bulk charge exchange lines.

The charge exchange lines are fitted by 4 Gaussian of H and D cold components and H and D hot components (I_H^{cold}, V_H^{cold} T_H^{cold}, I_D^{cold}, V_D^{cold} T_D^{cold}, I_H^{hot}, V_H^{hot} T_H^{hot}, I_D^{hot}, V_D^{hot}, T_D^{hot}, 12 free parameters). Here I, T, and V are intensity, flow velocity, and ion temperature, respectively. In order to reduce the number of the free parameters, the flow velocity, ion temperature, and D/H ratio of cold component ($V_H^{cold}=V_D^{cold}$, $T_D^{cold}=T_H^{cold}$, I_D^{cold}/I_H^{cold}, 5 parameters) are given by fitting the spectrum at beam off timing. The flow velocity of hot component is derived from the rotation velocity measurements of carbon impurity ($V_H^{hot}=V_D^{hot}=V_C^{hot}$, 3 parameters) and equal ion temperature between hydrogen and deuterium is assumed ($T_H^{hot}=T_D^{hot}$, 1 parameter). The amplitudes of hot and cold components, ion temperature, and D/H ratio of the hot components (I_D^{hot}/I_H^{hot}, $T_H^{hot}=T_D^{hot}$, $I_D^{hot}+I_H^{hot}$, $I_D^{cold}+I_H^{cold}$, 4 parameters) are selected as the free parameters to be fitted.

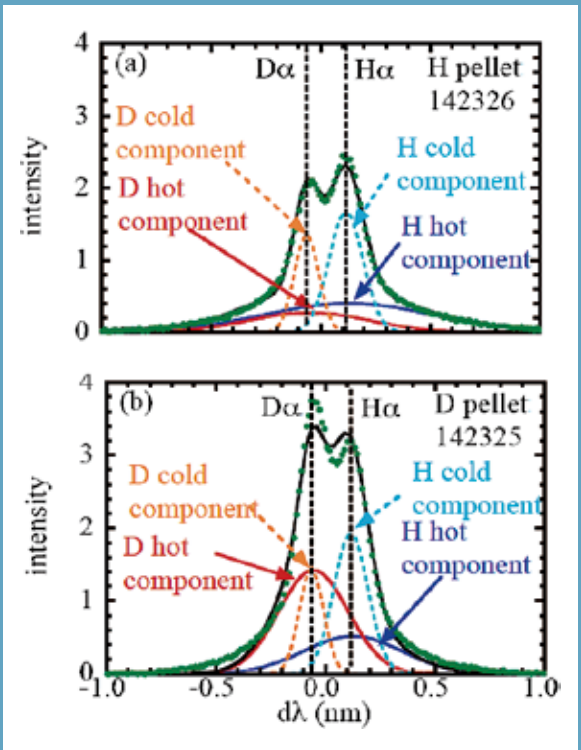

Fig. 1 Spectrum of H_α and D_α lines after H pellet and D pellet. The charge exchange lines are fitted by 4 Gaussian of H and D cold components (dotted lines) and H and D hot components (solid lines). Intensity (H hot component) > Intensity (D hot component) in the discharge with H pellet and Intensity (D hot component) > Intensity (H hot component) in the discharge with D pellet. There is almost no difference in cold components between the discharges with H pellet and D pellet, respectively.

Spectroscopic study of tungsten ions and hydrogen pellet ablation cloud

A spectroscopic study of tungsten ions has been carried out, for which the impurity pellet injection system is used to provide tungsten ions for the plasma. The measurement focuses on the pseudo-continuum radiation, the so-called UTA (unresolved transition array), of the tungsten ions, in particular. EUV (extreme ultra-violet) spectra including UTA in the wavelength range between λ = 15 Å and 70 Å are measured. From the temporal developments and spatial profiles of the UTA intensities, the charge states of ions responsible for several wavelength intervals in a UTA are identified as shown in Figure 2; λ = 49.24 Å to 49.46 Å by W^{27+}, λ = 48.81 Å to 49.03 Å by W^{26+}, and λ = 47.94 Å to 48.15 Å by W^{24+}.

A spatially resolved spectroscopic measurement inside the hydrogen pellet ablation cloud, which is elongated along the magnetic field line, has been conducted [2]. For that purpose, a band-shaped field-of-view is devised with optics composed of an optical fiber and a cylindrical lens. Spectra are continuously recorded when the ablation cloud crosses the field view so that the time series of spectra can be regarded as the spatial profile. The electron density n_e is evaluated from the Stark broadening of the H_β line for each spectrum (Figure 3) and the n_e profile in the ablation cloud along its elongation direction is derived. The obtained n_e profile is found to be peaked and have a dip at the center that is consistent with a simulation result [3].

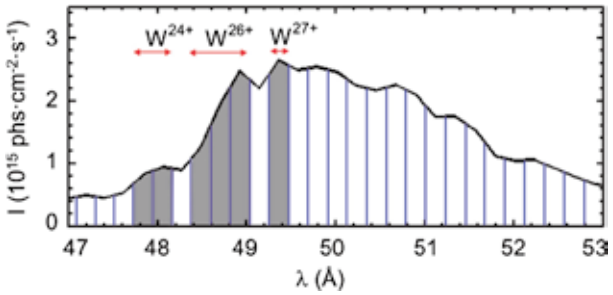

Fig. 2 Tungsten spectrum with UTA lines between λ = 47 Å and 53 Å. The three wavelength intervals indicated by the grey color are identified to be the UTA from W^{24+}, W^{26+}, and W^{27+} ions, respectively (cited from [1]).

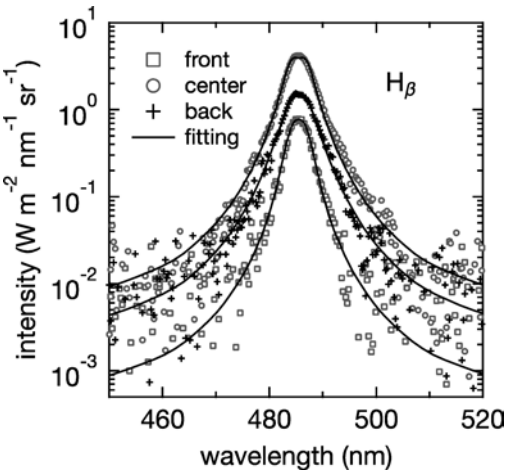

Fig. 3 Fitting results of the observed H_β line at different locations in the ablation cloud. The n_e at the front edge, center, and back edge are determined to be 1.2×10^{23} m^{-3}, 1.5×10^{23} m^{-3}, and 1.3×10^{23} m^{-3}, respectively (cited from [2]).

[1] Y. Liu *et al.*, J. Appl. Phys. **122**, 233301 (2017).
[2] G. Seguineaud *et al.*, Atoms **6**, 34 (2018).
[3] G. Cseh *el at.*, Nucl. Fusion **57**, 016022 (2017).

Study of nonlinear neutral beam-beam interaction effect in deuterium discharges

In the 19th experimental campaign, experiments in the plasma heating physics category such as feedback control of EC-wave polarization, 3rd harmonic ECH, effect of ECCD and NBCD on ion temperature, thermal equipartition between electrons and ions, nonlinear neutral beam-beam interaction effect, fundamental X-mode and EBW heatings, RF measurement using magnetic probe, ECE measurement using ECH antenna for optimum ECH and EBWH, collective Thomson scattering measurement, and others, were performed.

Here, we report the study of nonlinear neutral beam-beam interaction effect in deuterium (D) discharges. When two NBIs are operated with D and hydrogen (H) gasses with the same acceleration voltage, TASK/FP Fokker-Planck code predicts that the decay-time-constant of neutron yield, τ_D, after the stop of D-beam injection becomes longer when co-D-NBI and co-H-NBI are operated than τ_D in the case of co-D-NBI and counter-H-NBI. This prediction was experimentally confirmed. The agreement indicates that the slow D-ions are accelerated due to collision by faster H-ions in the case of both co-injection (Fig. 4).

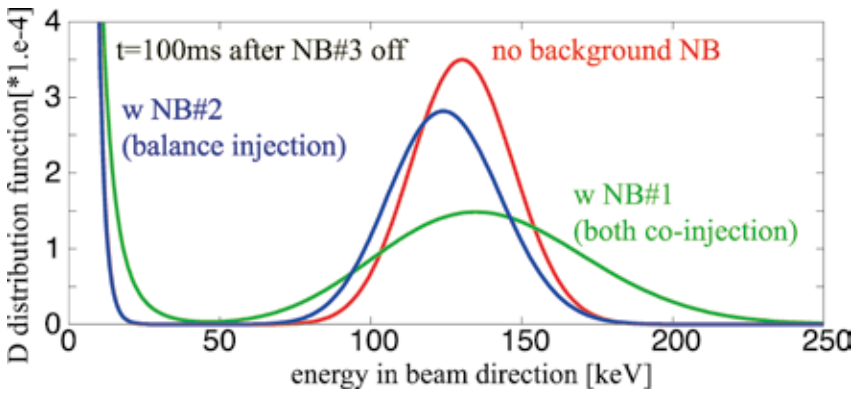

Fig. 4 Energy distribution functions of deuterium injected by NB#3 (co, D) in the cases of with NB#2 (counter, H), with NB#1 (co, H), and without other NBs.

Analysis of the tritium distribution on the wall

To confirm the overall tritium distribution on the wall surface, a tritium imaging plate (IP) technique was applied on the extracted first wall samples and divertor plate. Fig. 5 shows the representative IP images from the analyzed divertor tiles. The colored regions of the green and orange areas correspond to the density of the tritium distribution. The divertor strike point is often located on the bottom series of the tiles. On the other hand, the upper series of tiles, which perform the role of the baffle plate, shows a higher tritium level than that on the lower series. The standard tritium samples were placed on the IP together with the divertor tiles to estimate the relative density of the tritium on the tiles. The maximum tritium density can be roughly estimated in the near future. The mixed-material deposition layer mainly composed by carbon seems to be formed on the tile surfaces. Such a deposition layer might have acted as the possible tritium sink.

In the case of the first wall sample, the carbon based mixed-material deposition layers were clearly identified on the samples located at the outer side of the torus. Thick deposition layers were mainly found near the divertor tile arrays, and a high tritium level was detected on the deposition dominant region.

The carbon based mixed-material deposition layer seems to act as the main trapping site of the tritium. If the divertor tiles are replaced by metal materials, tritium inventory would be expected to be suppressed.

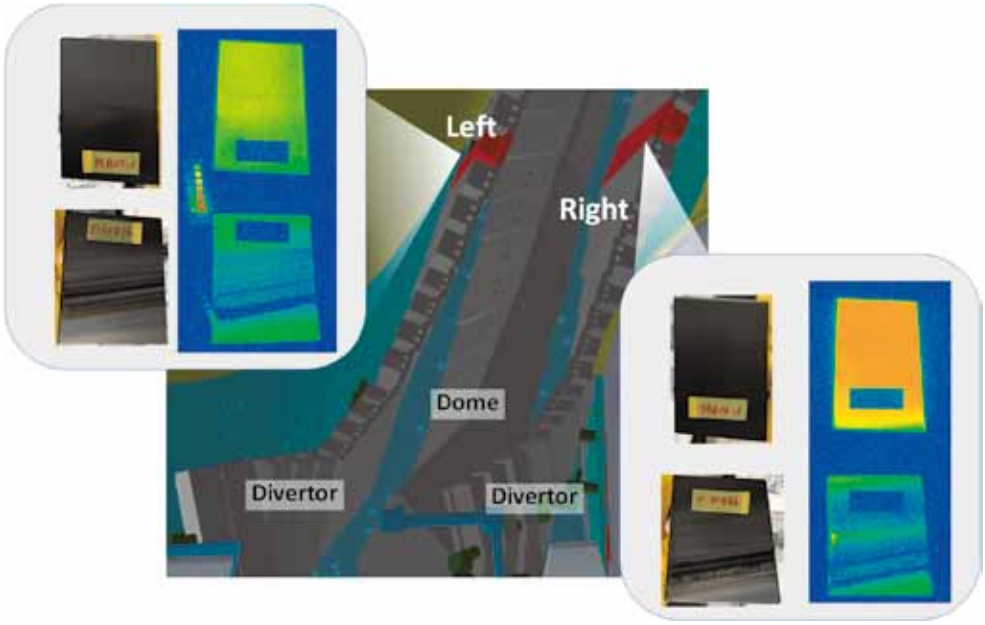

Fig. 5 The extracted divertor tiles and corresponding IP images from the left and the right hand side of the helical divertor array. The red colored tiles in the CAD image indicate the position of each tile.

Highlight

Isotope effects on confinement in ECRH plasma of LHD

The transport of different hydrogen isotopes is an important issue for predicting the performance of ITER and the future reactor operation. In a tokamak, improved transport character and lower H mode threshold power in D plasma than in H plasma were reported. Both tokamak scaling (ITER98y2) and helical scaling (ISS04) follow gyro-Bohm (GB) scaling with the exception of ion mass and ion charge number. While GB scaling predicts enhanced transport in D plasma, many experiments show better confinement (in tokamak) in D or comparable confinement (in medium-sized helical devices). In the 19th LHD experimental campaign, we performed the systematic study of the isotope effects in ECRH plasma of LHD.

In the dataset obtained in 19th LHD experimental campaign, the contamination of helium is less than 5% and the purity of the H and D are higher than 80%, respectively. The injection power was 0.6-3.9MW in D, 0.8-3.8MW in H, and $n_{e\ bar}$ was 0.6-3.7×$10^{19}m^{-3}$ in D, 0.3-3.8×$10^{19}m^{-3}$ in H. The one path absorption power was 92+-4% of injection power both for H and D plasma. Only one path absorption power was used for the τ_E estimation. The magnetic axis was 3.6m and Bt was 2.75T. Figure 1 shows comparison of predicted global energy confinement time (τ_E) by ISS04 scaling and experimental τ_E. The experimental τ_E was estimated from diamagnetic stored energy and power deposition calculated by LHDGAUSS [1]. As shown in Fig.1, τ_E in D plasma is systematically higher than τ_E in H plasma. The enhancement factors are τ_E / $\tau_{E_{ISS04}}$=1.27+-0.12 in D and 1.09+-0.02 in H plasma. Thus, improvement of τ_E in D to H is 17%. The regression analysis was performed, then, the scaling $\tau_{E\ ECH} \propto A^{0.24\pm0.01} n_{e\ bar}^{0.58\pm0.01} P_{abs}^{-0.52\pm0.01}$ were obtained, where A is ion mass (1 for H, 2 for D), $n_{e\ bar}$ is the line averaged density, and P_{abs} is absorption power. The power exponent of A, which is 0.24, is a similar value to tokamak L mode scaling.

The contribution of the neoclassical heat flux is around one-half of the total heat flux. The improvement is due to the reduced turbulence driven transport [2]. The clear improvement of core electron transport was found in electron ITB plasma [3]. The detail investigations of the turbulence characteristics are now underway from the turbulence measurements and gyrokinetic analysis.

[1] T. Tsujimura *et al.*, Nucl. Fusion **55** (2015) 123019.
[2] F. Warmer *et al.*, Nucl. Fusion **58** (2018) 106025.
[3] H. Takahashi *et al.*, Nucl. Fusion **58** (2018) 106028.
[4] H. Yamada *et al.*, Nucl. Fusion **45** (2005) 1684.

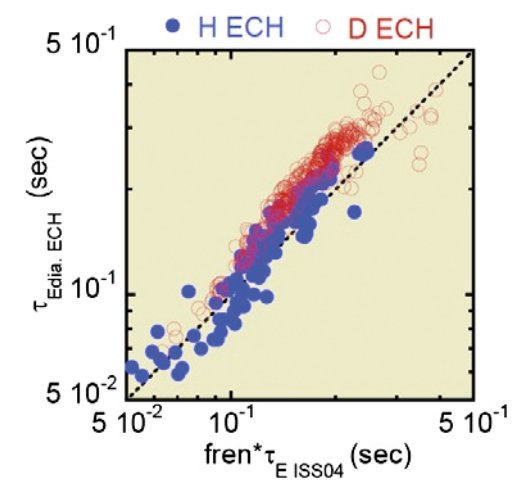

Fig. 1 Comparison of ISS04 prediction and experimental global energy confinement time. fen is the normalization factor of ISS04 scaling [4].

Observations of rapidly varying radial structure of flow velocity around spontaneously rotating magnetic island

The radial profile of flow velocity can be observed by newly installed microwave frequency comb Doppler reflectometer when the spontaneous rotation of magnetic island occurs. Because the spontaneous large sized magnetic island sometimes leads the plasma collapse in the LHD, the understanding of the physical mechanism is one of the important issues.

Doppler reflectometer gives the temporal behavior of perpendicular flow velocity $V_\perp$. This flow velocity and also the radial electric field are well known to affect the growth and decay of the magnetic island. In the experiment, it is clearly observed when the m/n=1/1 magnetic island is rotating, $V_\perp$ is oscillating at the same frequency as the magnetic fluctuation, as shown in Fig. 1. The value of $V_\perp$ changes back and forth from around -10 to 0 km/s until t=5.185 s. The observed change of the two values could be explained as follows from the knowledge of the past LHD experiments which showed that the poloidal velocity in the static magnetic island is almost 0 km/s. The observation of $V_\perp \sim 0$ km/s means that the O-point of the rotating magnetic island comes to the observation region. On the other hand, when the O-point of the magnetic island is absent in the observation point, the value of $V_\perp$ equals the background flow velocity. Then, the signal oscillates between two values. This suggests that the Doppler reflectometer can measure the structure of fast varying magnetic island. Figure 2 shows the temporal change of the radial profile of the $V_\perp$. Periodically, $V_\perp \sim 0$ (green color) appears widely in the plasma edge region. Although the center position of the magnetic island is the core region (r_{eff}/a_{99}~0.7), the observation results clearly show that the effect of the island structure extends over a wide range. These results are quite meaningful to understand the spontaneous rotating magnetic island affecting the confinement.

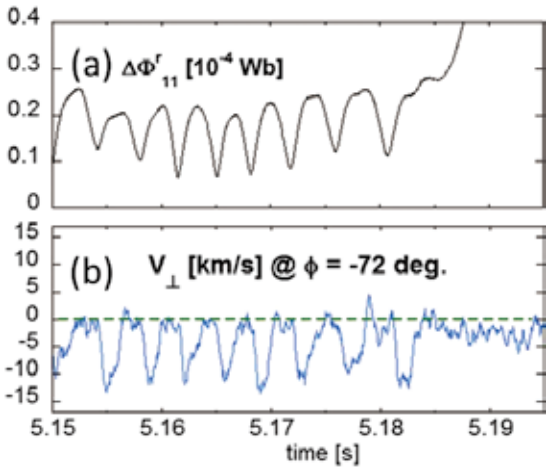

Fig. 1 Temporal change of (a) m/n=1/1 component of the radial magnetic flux and (b) the perpendicular velocity around r_{eff}/a_{99}=0.96. Cited from Fig. 3 in [1].

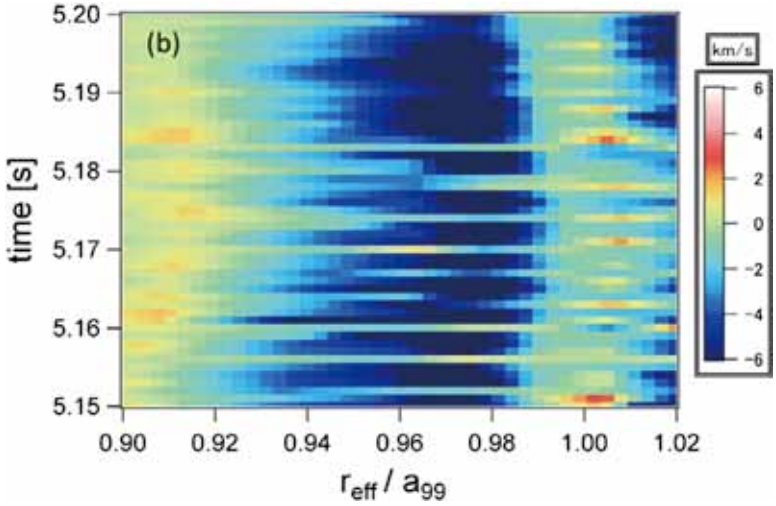

Fig. 2 Spatio-temporal behavior of $V_\perp$ in the plasma edge region. Here, r_{eff} is the effective minor radius and a_{99} is the effective minor radius of which encloses 99% of the total electron pressure. Cited from Fig. 4 in [1].

[1] T. Tokuzawa *et al.*, Nucl. Fusion **57** (2017) 076003.

Helically trapped energetic particle driven resistive interchange mode (EIC)

Repeated bursts of the magnetic fluctuations were observed in the hydrogen campaign of LHD in the low electron density regime [1]. This activity is called helically trapped Energetic particle driven resistive InterChange modes (EIC), since the pressure gradient of helically trapped energetic particles (EP), shown in Fig. 4, drives this mode. Helically trapped EPs are mainly produced by the perpendicularly injected beams. Two perpendicular neutral beam injection (PERP-NBI) systems are upgraded for the deuterium plasma campaign, and the injected power increases from 6+6 MW to 9+9 MW, respectively. As results, the beta value of helically trapped EPs, $\beta_{\perp}$ has increased up to $\beta_{\perp}$~0.35 %. And it is found that the amplitude of the EIC bursts becomes larger in the deuterium campaign as shown in Fig. 2 [2].

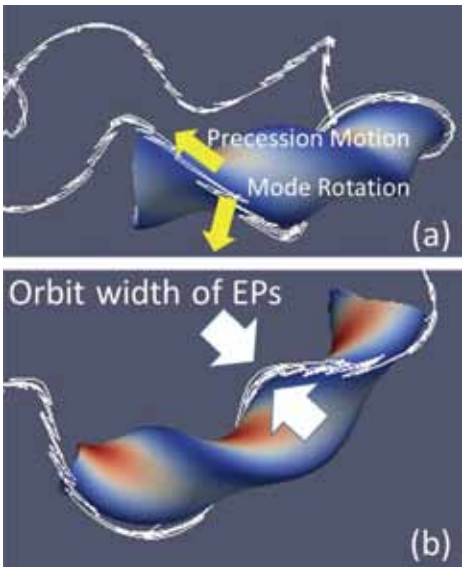

Fig. 1 Orbit of the helically trapped particle. The surface color indicates the magnetic field strength.

Excitation of the EIC requires resonance of the precession motion of the helically trapped EP and the MHD mode. In the deuterium experiments with higher beam energy, the effect of the EP becomes smaller because the orbit width of EPs (Fig. 1(b)) is wider and the EPs stay a shorter time inside the eigenfunction of the resistive interchange mode. Therefore, since the EIC mode is more stable with D beam, the energetic particle pressure becomes larger before each EIC burst. That is the reason why the EICs are excited less frequently and with a larger amplitude.

The effects of the EIC on the performance of the plasma is not negligible (Fig. 2(b)). Therefore, several controlling methods, based on the physical mechanism of the EIC, are being tested. One promising candidate is the EC heating. When the electron temperature around the rational surface increases, the width of the eignenfunction narrows. The interaction between EPs and the MHD mode is thereby reduced. Disappearance of the EICs and the performance enhancement are observed with EC heating.

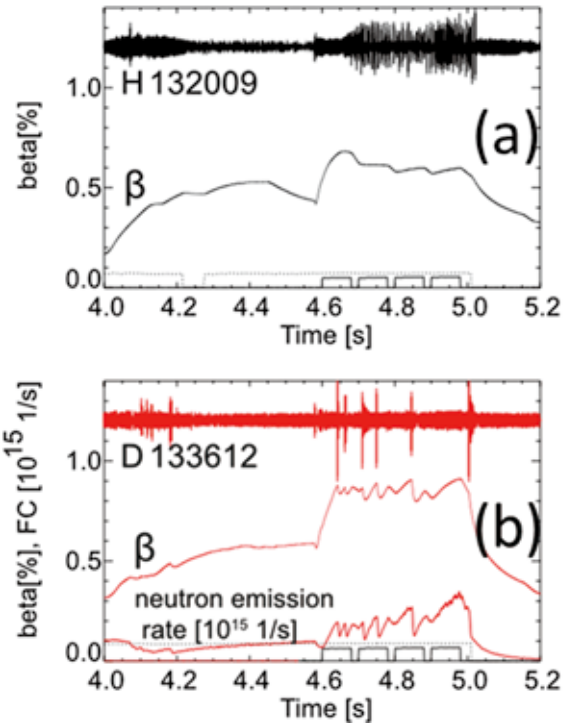

Fig. 2 Time evolution of the magnetic fluctuations with H beam (a) and D beam (b). Time evolution of the diamagnetic beta value and the neutron emission rate (only with D- beam) are shown together.

[1] X. D. Du, *et al.*, Phys. Rev. Lett, **114** (2015), 155003.
[2] T. Bando, *et al.*, Nucl. Fusion, in press.

Dependence of RMP penetration threshold on ion species in helical plasmas

The intrinsic RMP (error field) is thought to be a cause of tokamak disruption induced by the locked mode instability, and the RMP by external coils is applied as an effective control knob to improve the confinement performance in the torus plasmas. However, it is reported that the RMP is sometimes shielded by plasmas, and it penetrates plasmas when the amplitude of the RMP is larger than a value, which is called the penetration threshold. The phenomena are observed in both tokamaks and in helicals, including the LHD.

The most popular model on the shielding mechanism of the external RMP is a balance between the electro-magnetic and the viscous torque [1]. According to a model [2] in helical plasmas without an external torque, the poloidal neoclassical viscosity is considered dominant, and the viscous torque is expressed by the product of a poloidal rotation speed and a viscosity coefficient, and the electro-magnetic one is roughly proportional to the square of the RMP coil current.

Since it is expected that the plasma rotation speed depends on the ion species, we compare the m/n=1/1 RMP penetration threshold in the hydrogen and the deuterium plasmas. Figure 1 shows the threshold dependence on the collisionality in the hydrogen and the deuterium of the LHD with A_p=5.7 and β_{local}~0.3%. Here A_p is the plasma aspect ratio. From Fig. 1, the penetration threshold in the deuterium is smaller than that in the hydrogen, which means that we can affect the plasmas by the smaller RMP in the deuterium than in the hydrogen. In Fig. 2, we plot the penetration thresholds of theVarious aspect ratio, beta, and ion species plasmas (A_p=7.1; ◇, A_p=5.7; ○ and H; ●, D; ■) as the function of the plasma poloidal rotation ($\omega_{pol@t=1}$) at the rational surface just before the penetration. In all of the cases, the RMP penetration thresholds are higher as the poloidal rotation is faster, which is qualitatively consistent with the torque balance model between the electro-magnetic and the poloidal neoclassical viscous torque [2]. Then the main reason why the penetration threshold in the deuterium is lower than that in the hydrogen is considered to be because the poloidal rotation in the deuterium is slower than that in the hydrogen.

[1] R. Fitzpatrick, Nuclear Fusion **39** (1993) 1049.
[2] S. Nishimura *et al.*, Phys. Plasmas **19** (2012) 122510.

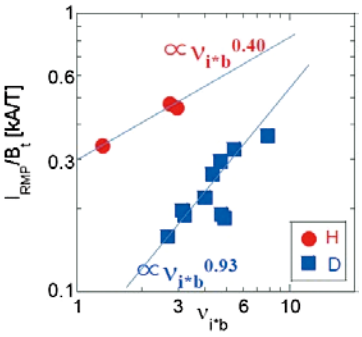

Fig. 1 RMP penetration threshold as the function of the collisionality in the LHD with A_p=5.7 and β_{local}~0.3%.

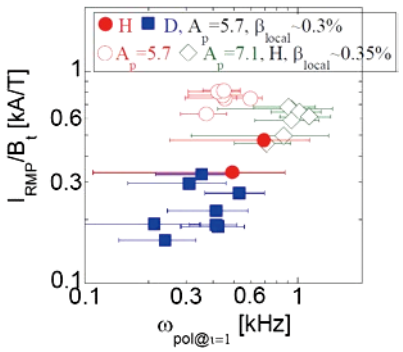

Fig. 2 RMP penetration threshold as the function of $\omega_{pol@t=1}$ in the LHD with A_p=5.7~7.1 and β_{local}=0.3~0.35%.

(T. Morisaki)

Research and Development collaboration program for LHD-project

A special collaboration program, which is aimed to support the research and development activities in domestic universities for advanced diagnostics or heating scenarios, is founded for the future application on LHD. Two examples of such activities are shown in this section.

a) Development and Installation of Electron Cyclotron Emission Imaging Diagnostics

Imaging diagnostics using microwave has been made remarkable contribution to the research on MHD instabilities and turbulence studies in large devices [1]. Over the past few years, we have been proactively developed the microwave imaging devices under the collaboration between NIFS and the Tokyo University of Agriculture and Technology. Based on these activities, a new electron cyclotron emission imaging (ECEI) system was successfully developed for LHD and started its operation during the LHD experiment campaign in 2017. The observation frequency of this ECEI system is 50~57 GHz (2nd harmonic), and this system has 8 channels in each of poloidal and radial directions (frequency domain). One of the key device in this ECEI system is a new antenna array, which is named as Local oscillator Integrated Antenna array (LIA) as shown in Fig. 1 [2,3].

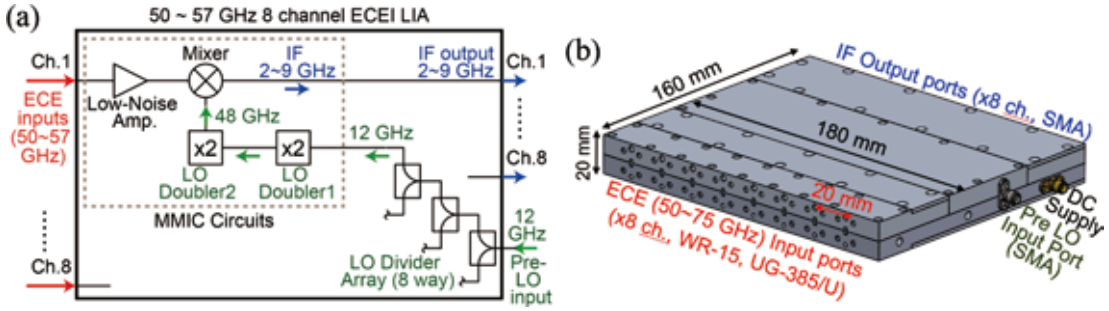

Fig. 1 (a) Schematic diagram of LIA circuit, and (b) outside drawing of LIA.

The role of this antenna array is to convert very high frequency ECE signals (need to be treated as light) to cable-transmittable low Intermediate Frequency (IF) signals using a mixer and Local Oscillation frequency (LO). A conventional ECE antenna array requires special LO optics, where the uniform LO power feeding to each antenna element is difficult. It also requires an expensive high-power LO source. Our new LIA has successfully solved these problems using a microwave monolithic integrated circuit (MMIC) as LO supply unit, which is installed at each antenna element. Using compact and inexpensive MMIC frequency multipliers, it became possible to supply the low frequency Pre-LO signal to the LIA via a coaxial cable.

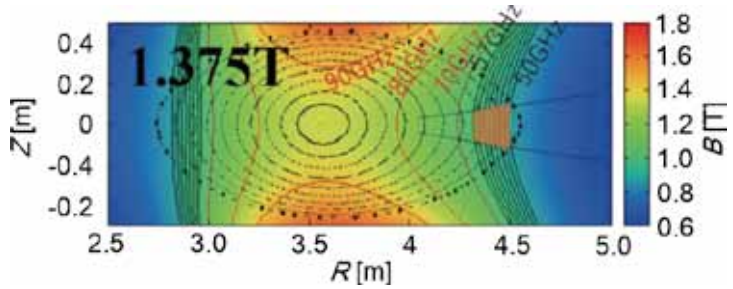

Fig. 2 The observation area of 50~57 GHz ECEI system at B_t = 1.375 T [4].

The observation area of our new ECEI system, which is installed at the 4-O port of LHD, is shown in Fig. 2, where the magnetic field strength on axis is set to 1.375 T. The focal point of the optics is located near the outer half radius of the LHD-plasma to detect the oscillation on the ι = 1 (m/n = 1/1) surface.

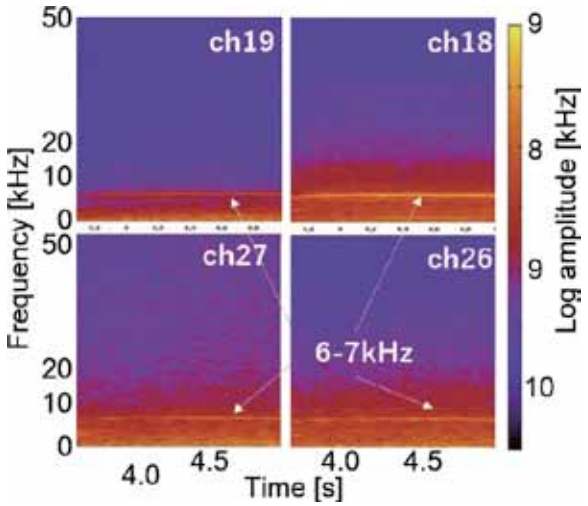

Fig. 3 Time evolutions of frequency spectrograms of ECE signals for Ch19 (52GHz), ch27(52 GHz), ch18(51GHz) and ch26(51 GHz), respectively [4].

Figure 3 shows the time evolutions of frequency spectrograms of the ECE signals from selected channels from this ECEI system. The fluctuation between 6 and 7 kHz was observed in each channel. It was evaluated from the toroidal and poloidal mode analysis by a magnetic probe array that the fluctuation was due to the MHD instability around ι = 1 surface, The phase difference between each ECEI channel was also evaluated, and the propagation direction and the correlation length can be estimated.

[1] H. Park *et al.*, Rev. Sci. Instrum. **75** (2004) 3875.
[2] D. Kuwahara *et al.*, Rev. Sci. Instrum. **85** (2014) 11D805.
[3] Y. Nagayama *et al.*, Rev. Sci. Instrum. **88** (2017) 044703.
[4] H. Tsuchiya *et al.*, Plasma Fusion Res. **13** (2018) 3402063

b) Development of plasma diagnostics for detached plasmas

To improve the core plasma performance, it is inevitable to understand the physics in divertor region as well as core plasmas. Plasma detachment is thought of as a method to control particle/heat loads on divertor materials; the measurement of the low temperature recombining plasmas is not so simple. Anomaly is identified in the current voltage characteristics of electrostatic probes, and a special care is required for Thomson scattering, since the temperature is much lower than 1 eV. In this study, based on developments of measurements systems in linear divertor simulators, the understanding in the physics of plasma detachment was progressed. A Tunable Diode Laser Absorption Spectroscopy (TDLAS) and a Laser Thomson Scattering (LTS) system have been developed to measure the atomic temperature and the electron density and temperature in the divertor simulator NAGDIS-II.

A TDLAS system was developed using a distributed feedback (DFB) laser. TDLAS of helium metastable (23S1) has been carried out using a lab-made DFB laser system in the detached plasma 1.4 m downstream from the discharge region [5]. Figure 4 shows the non-averaged absorption spectra of metastable helium atoms in a detached plasma. The Gaussian fitted lines were obtained using the spectra averaged over repeated measurements. The temperature and density of the metastable helium atom were derived as 0.04 eV and 1.6×10^{17} m^{-3} from the width and area of the absorption coefficient spectra, respectively.

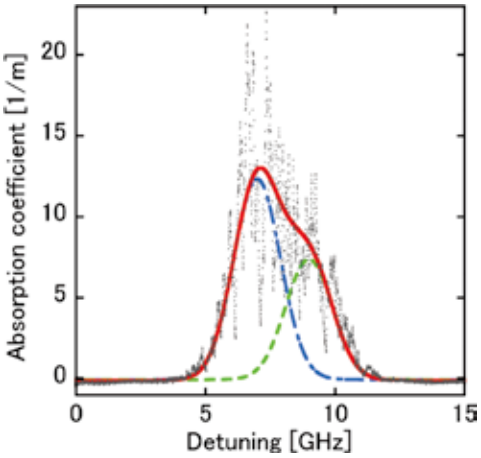

Fig. 4 Non-averaged absorption spectra in NAGDIS-II (from [1]).

An LTS system was developed for the NAGDIS-II using an Nd:YAG laser (Continuum: SLII-10) at the wavelength of 532 nm with the pulse width of 5-6 ns. The spectrometer is composed of a volume phase holographic grating (2600 l/mm) and two camera lenses [6]. The high etendue spectrometer was developed based on prototypes for MAGNUM-PSI [7]. Figures 5(a) and (b) show typical Thomson scattering (TS) spectrum in an attached ionizing plasma and a detached recombining plasma, respectively. To obtain the spectrum, TS signals were averaged 300 times (30 s). The plasma parameters were successfully deduced from the spectrum. The deduced temperature in the detached plasma was 0.29 eV, which was one order of magnitude lower than the attached plasma.

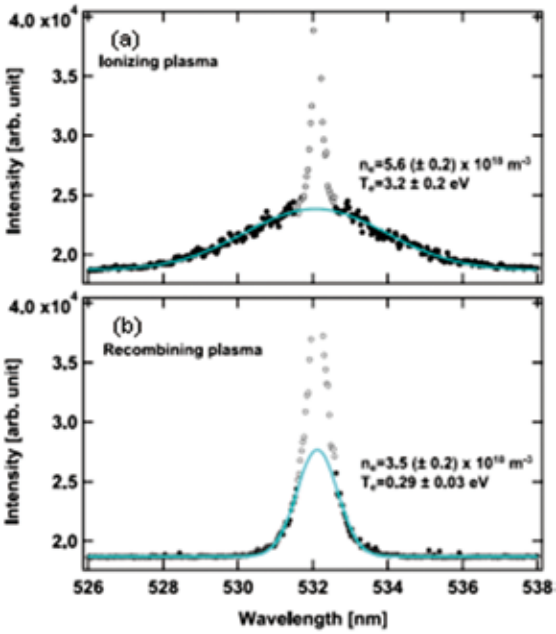

Fig. 5 Typical TS spectrum in (a) an attached ionizing plasma and (b) a detached recombining plasma, respectively (from [6]).

From the TDLAS and LTS measurements, it was found that metastable state atoms were produced in the peripheral region of the plasma and transported toward the wall radially. It was also revealed from the detailed LTS spectrum analysis that the plasma had two electron temperature components, and the values were consistent with those obtained from the helium line intensity ratios method [8]. Those results suggested the importance of future investigation in the influences of transport of metastable state atoms and fluctuations on line emission in recombining plasmas.

[5] M. Aramaki, T. Tsujihara, S. Kajita, H. Tanaka, and N. Ohno, AIP Advances, **8** 015308 (2018).
[6] S. Kajita, T. Tsujihara, M. Aramaki, *et al.*, Phys. Plasmas **24**, 073301 (2017).
[7] H. J. van der Meiden, A. R. Lof, M. A. van den Berg, *et al.*, Rev. Sci. Instrum. **83**, 123505 (2012).
[8] S. Kajita, K. Suzuki, H. Tanaka, N. Ohno, Phys. Plasmas **25**, 063303 (2018).

(M. Osakabe)